ISIJ International, Advance Publication by J-STAGE, DOI: 10.2355/isijinternational.ISIJINT-2021-498

Effect of Different Remelting Parameters on Slag Temperature and Energy Consumption during ESR

Reinhold SCHNEIDER,[1)]* Valentin WIESINGER,[1,2)] Siegfried GELDER,[3)] Alec MITCHELL[4)] and Daniel DAVID[1)]

1) Univ. of Appl. Sciences Upper Austria, Wels, Austria.
2) K1-MET GmbH, Linz, Austria.
3) voestalpine Böhler Edelstahl GmbH & CoKG, Kapfenberg, Austria.
4) Univ. of British Columbia, Vancouver, Canada.

(*Received on November 7, 2021; accepted on January 14, 2022; J-STAGE Advance published date: March 16, 2022*)

Energy consumption is a vital aspect in the production of high quality materials by using electro slag remelting as a refining method. The electrical conductivity and the melting point of the slag, determined by the slag composition, as well as the fill ratio, the amount of slag and the melt rate have as significant influence. Several of these factors as well as a new method to measure the slag surface temperature with a two-color pyrometer were investigated in laboratory scale remelting trials. Two different slags with an average and a low electrical conductivity were used. While there is only a small impact of the slag cap height and the melt rate, the slag composition showed a strong effect, both on the slag surface temperature as well as on the specific energy consumption. Additional investigations confirmed that the effect of the slag composition on the amount and compositions of non-metallic inclusions, respectively the cleanliness level of the steel after remelting is rather minor. The results suggest possibilities for easily applicable, improved process parameters, which can combine high product quality with significantly reduced energy consumption.

KEY WORDS: electro slag remelting; slag temperature; energy consumption; non-metallic inclusions.

1. Introduction

1.1. Parameters Affecting Energy Consumption in ESR

The specific energy consumption has been an important topic from the beginning of ESR investigations (*e.g.*[1,2)]). Results documented in these sources as functions of current and voltage for a laboratory scale ESR-unit in 1) range from 1 000 to over 2 000 kWh/t and 880 to 1 600 kWh/t in 2). In standard works on ESR *e.g.*[3)] the quoted energy consumption for steels is often generalized to the range of 1 000–1 500 kWh/t and was widely accepted as a fundamental factor of this technology. However, the rising awareness and the regulatory requirements regarding sustainability, environmental protection and emissions control along the entire process chain have recently activated new awareness for this topic.[4,5)] Based on data in 4), estimating the total annual ESR production with 2 million tons, and assuming a rather optimistic average energy consumption of 1 000 kWh/t, ESR accounts for at least 2 TWh in annual consumption of electric energy worldwide.

Besides plant design and geometrical conditions, the slag plays the key role in the heat generation and energy consumption of ESR and is usually CaF_2-based. Key properties are the electrical resistivity in the liquid state (which is directly connected to the viscosity), the melting point (which needs to be adjusted to the melting point of the metal), and the electrical and thermal conductivity, especially in the slag skin between the ingot and the mold.[2,6)] Slag compositions are easy to change from one melt to the other independent from the plant design and therefore provide a simple tool to affect energy consumption. Furthermore, low-CaF_2 containing, high-resistivity slags contribute to reduced fluorine pollution.[5)] Through other factors such as fill ratio and the amount of slag or the melt rate can also have a strong effect.[4)] Such factors need to be taken into consideration when evaluating and comparing different results.

The subsequently evaluated data are depicted in two separate diagrams, one for lab-scale setups in **Fig. 1**(a) and one for (semi) industrial plants with a mold diameter of at least 300 mm in Fig. 1(b). Data from 7), 8) and 9) are based on measured electrical conductivity values at 1 600°C of the respective slags. The electrical conductivity of the other data points in Fig. 1 are calculated values for 1 600°C, using the chemical compositions of the quoted sources and Eqs. (1) and (2) from 10) whereby the electrical conductivity κ is:

$$\kappa = exp^{(1.911-1.38N_x-5.69N_x^2)} + 0.0039.(T-1700) \quad \text{..... (1)}$$

* Corresponding author: E-mail: r.schneider@fh-wels.at

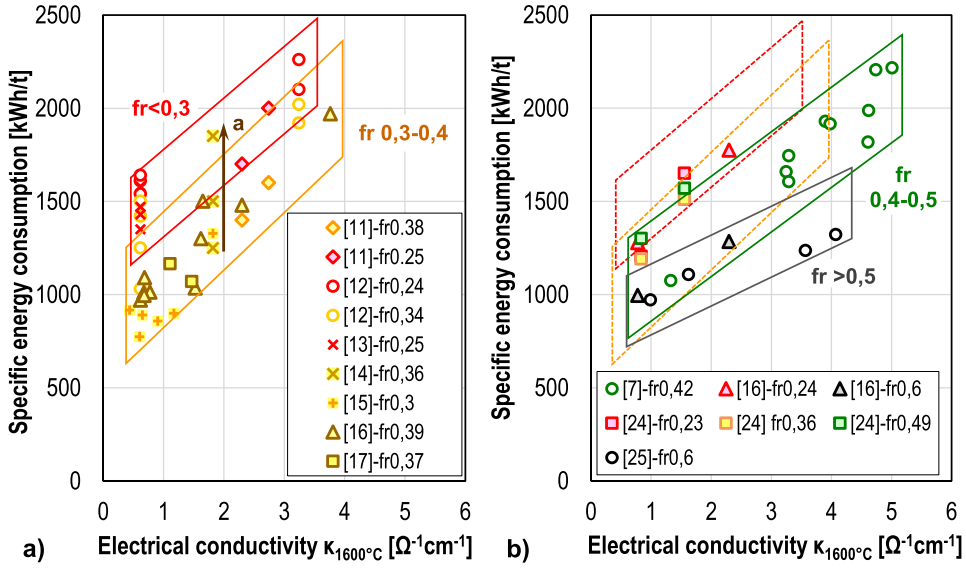

Fig. 1. Specific energy consumption as a function of the electrical conductivity at 1 600°C for a) laboratory scale experimental ESR units and b) semi-industrial and industrial ESR plants. (Online version in color.)

N_x represents the weighted mole fraction of the different slag components.

$$N_x = N_{Al_2O_3} + 0.75N_{SiO_2} + 0.5(N_{TiO_2} + N_{ZrO_2}) + 0.2(N_{CaO} + 2N_{CaS}) \quad \text{..... (2)}$$

and T is the temperature in °C.

To distinguish the effect of the electrical conductivity from other factors, the fill ratio "fr" ($D^2_{electrode}/D^2_{mold}$) was used as an indicator in Fig. 1 using red symbols for fr < 0.3 yellow-brown for fr = 0,3–0.4, green for fr = 0.4–0.5 and grey-black for fr > 0.5. Most energy consumption data published are from small scale experimental ESR-plants (Fig. 1(a)).

Laboratory experiments (mold diameter 100 mm) conducted with a construction steel, two different fill ratios of 0.25 and 0.38 and two different slag compositions (CaF_2/CaO/Al_2O_3) of 70-0-30% and 60-20-20% show an approx. 20–25% increase in specific energy consumption due to the reduction of the fill ratio and about 15% increase due to the lower resistivity.[11] Similar effects of different fill ratios (0.24 and 0.34), slag compositions (CaF_2/CaO/Al_2O_3) of 70-15-15% and 0-50-50% and two different steels (C–Mn-steels and an austenitic stainless steel) are documented for laboratory investigations with two different ESR-units.[12] The variations include also alteration of the amount of slag, current, voltage and the melt rate, making a clear differentiation of the various factors challenging. Specific energy consumption covers the whole range from 1 030 to 2 260 kWh/t. For the best comparable parameters, the use of the high resistivity CaF_2-free slag reduces the specific energy consumption compared to the low resistivity slag by about 25–35%. The second clear effect is a 10–20% higher consumption value by using the lower fill ratio, but lower fill ratios were exclusively used in the stainless steel work therefore an effect of the electrode material cannot be excluded.

Data on energy consumption can also be found in 13) for a laboratory ESR unit operated with a mold diameter of 100 mm and fill ratio of 0.25, stainless steel electrodes and a CaF_2-free slag with 50% CaO and Al_2O_3 each. The average energy consumption between 1 350 and 1 580 kWh/t is typical for this low fill ratio. The lower value is mainly the result of an increased melt rate. The results of experiments with the same mold diameter, a carbon steel and a filling ratio of 0.36, using various amounts (1.3, 1.8 and 2.4 kg) of a CaF_2-based slag (30% CaO and Al_2O_3) are reported in 14). The data show a strong increase of the specific energy consumption with rising slag quantity, ranging from about 1 250 to roughly 1 850 kWh/t, an almost 50% increase. This variation is indicated in Fig. 1(a) with yellow "x"-marked data points and a brown arrow designated "a". Additionally, the energy consumption was found to be almost independent from the melt rate. Comprehensive lab scale investigation with a 155 mm mold and a fill ratio of 0.27–0.3 with various, mostly CaF_2-free slags using a ball bearing steel lead to energy consumptions in the range of 800–1 300 kWh/t in the stationary part of the remelting process.[15] All CaF_2-free slags were found to lead to consumption below 1 000 kWh/t, confirming the particular advantage of such slags.

A systematic investigation covering a wide range of slag composition on a laboratory scale ESR unit with a mold diameter of 120 mm and a fill ratio of 0.39 can be found in 16). The results demonstrate the strong effect of the electrical conductivity on energy consumption with the highest values of 1 970 kWh/t being double the lowest values. Energy consumption values of about 1 000 kWh/t or below can thus be achieved with low or no CaF_2-containing slags as well as with slag containing combined high amounts of Al_2O_3 and SiO_2. The effect of increased SiO_2-contents on the specific energy consumption at otherwise similar experimental conditions on a laboratory ESR unit (mold diameter 168 mm, fill ratio 0.37) in 17) shows a slight increase with rising SiO_2 content. As SiO_2 is a component which is increasing the resistivity, this result is contradicting the general trend, indicating the effect of other factors. However, the differences are in the typical scatter band.

Lab scale experiments with a mold diameter of 127 mm but unknown fill ratio in 18) extend the results from a slag with average resistivity (1 200 kWh/t) to pure CaF_2 with best conductivity resulting in an energy consumption up to 1 900 kWh/t, an almost 60% increase. This effect may be partially the result of a change in the slag heat balance due to a change in the slag thermal conductivity from a phonon mechanism in low-CaF_2 slags to one of photon conductivity

in high-CaF_2 compositions.[19)]

Energy consumption for the lab scale remelting of two Ni-base-alloys and one bearing steel reported in 20) for general ESR operation ranges from 1 265 to 1 587 kWh/t. This value can be reduced to 735–924 kWh/t by an additional electrode, acting also as thermal barrier in the upper part of the mold. However, this technique has not found significant industrial application.

Switching to production data, the effect of the plant size described in 21) shows a continuous increase from surprisingly low values of about 600 kWh/t for a 1-ton plant, to 1 800 kWh/t at a large, more than 200-tons ESR unit. Furthermore, towards higher plant sizes, most processes tend to have a low fill ratio or use multiple (3 or 4) electrodes which are equivalent to a low fill ratio. However, no data are stated for a more detailed evaluation. Experiments with a semi-industrial size plant, mold diameter 300 mm and fill ratio 0.59, comparing AC with both types of DC-operation using a unspecified CaF_2–Al_2O_3–CaO-slag show an advantage of "DC-Straight Polarity" (860 kWh/t) over AC (1 070 kWh/t) at the expense of a significantly reduced quality.[22)] In contrast, "DC-Reverse Polarity" gave similar ingot quality but higher energy consumption of 1 290 kWh/t. This value rose to 1 430 kWh/t when the fill ratio was lowered to 0.44 using a slag cap height of 100 mm in all these cases. A strong dependency on the slag cap height was observed at this fill ratio, lowering the energy consumption to 1 290 kWh/t at 75 mm and increasing it to 1 800 kWh/t for 125 mm slag cap height, a difference of 40%. Similar experiments on a larger scale plant (mold diameter 430 mm) using slag compositions (CaF_2/CaO/Al_2O_3) of 40-30-30% in 23) gave a value of 1 000 kWh/t for AC-operation, 900 kWh/t for "DC-Reverse Polarity" and 1 600 kWh/t for "DC-Direct Polarity". (However, the denoted information on the oxygen content indicates an inverse use of the terms for "DC Polarity").

Low fill ratios (<0.2) were also identified as a major factor to increase specific energy consumption in 24) for two different slags (CAF1 and CAF3) with high resistivity using a semi-industrial mold size of 300 mm. Thereby a strong effect of the slag resistivity can be seen (Fig. 1(b)). The results indicate that fill ratios up to about 0.4 lead to reduced energy consumption due to a better heat transfer into the electrode and less radiation losses at the free slag surface. Higher fill ratios surprisingly resulted in slightly increasing energy consumption, which is against the general trend found in other sources. This behavior was justified by specific experimental conditions due to changing immersion depths. Laboratory experiments and also industrial production scale results can be found in 16). While the fill ratio of the lab scale was 0.39 the industrial scale varied between 0.24 and 0.6 depending on the electrode size used. The results from different higher alloyed steel grades confirm that the fill ratio is the dominant size factor, resulting in changes in energy consumption of 28 to 38%, rather than the plant size. The results also demonstrate the strong effect of the electrical conductivity. Energy consumption vales below 1 000 kWh/t can thus be achieved at higher fill ratios combined with low or no CaF_2-containing slags. Recent reports of systematic research on energy consumption in ESR on the industrial scale are rare. A comprehensive investigation using a wider variation of slags with different measured electrical conductivities but similar melt rates and its impact on the specific energy consumption using the same technical equipment (mold diameter ~400 mm) and electrode materials (martensitic stainless steels) is documented in 8), 9) and more extensively in 7). With a focus on rather unusual high CaF_2-containing slags, the parameters cover a wide field of conductivity at a fill ratio 0.42 and demonstrate a clear correlation with the energy consumption. Compared to a commercial slag with about 1/3 CaF_2, CaO and Al_2O_3 each, the almost pure CaF_2-slag doubles energy consumption. A particular advantage of this investigation is the circumstance that electrical conductivities of the slags used were not calculated by regression formulas, but determined by experimental methods.

Some of the few documented large scale experiments with a mold diameter of 800 mm, an equal melt rate and a fill ratio of 0.6 can be found in 25). Using slag composition with a wide variety of CaF_2 contents, the fundamental correlation between electrical conductivity and specific energy consumption is apparent but with a less massive rise compared to the other sources (Fig. 1(b)). The high fill ratio appears to negate the effect of a high conductivity slag.

Figure 1(a) shows the strong tendency of rising energy consumption with increased conductivity, however the effect of the fill ratio (accentuated with red and yellow frames) indicates the importance of this factor. High fill ratios are difficult to achieve in small experimental units as a certain distance between the electrode and the mold has to be maintained. The relatively wide areas covered by the frames and its overlap demonstrate that other factors, such as specific plant characteristics, melt rate, slag cap height *etc.* cannot be neglected as relevant, but their importance changes from source to source. These frames were transferred to the Fig. 1(b) and show good conformity with (semi) industrial scale results. Therefore energy consumption data from experimental investigations can well be transferred, particularly when lab scale experiments are conducted with the largest fill ratios possible. The areas for results with higher fill ratios are also marked with green and dark grey frames, demonstrating the potential for energy savings at high fill ratios.

1.2. Factors Affecting Slag Skin Thickness

Slag skin thickness values, as a main factor limiting the heat transfer to the mold, are sparsely documented. For DC-operation values of "<1.6" mm to "3.2+" mm with rising slag cap height are reported.[22)] Data in 26) from lab-scale experiments document slag skin thickness of 0.8–1.2 mm using different process parameters. A variation of slag temperatures using pure CaF_2 in 27) show a strong effect on the slag skin thickness ranging from 4.4 mm at 1 460°C slag temperature to 1.02 mm at 1 720°C. Changing the slag system from pure CaF_2 to CaF_2 + 25% Al_2O_3 at a similar slag temperature of about 1 650°C almost tripled the slag skin thickness, which may also be an indication of the change in slag thermal conductivity mechanism as oxide is added to pure fluoride.[19)] However, an in-depth analysis of the corresponding overall heat transfer coefficient indicates, that the effect of the slag temperature and the related slag skin thickness is only in the range of about 30%.[2,27)]

A strong influence of the slag temperature on the thickness of the slag skin was also documented in 28) for two different slags. In this work the CaF_2-based slag containing 30% Al_2O_3 could be operated a 50°C higher slag temperature to achieve the same slag skin thickness of 2 or 3 mm than the CaF_2-based slag containing 20% CaO and 20% Al_2O_3, which might partly be explained by different melting points. Furthermore, it is pointed out in 28) that the slag skin

thickness needs to be balanced between ensuring a smooth ingot surface and sufficient heat transfer to avoid deep liquid metal pools.

Measurements on the slag skin thickness with a wide variation of process parameters using the same slag (60% CaF_2/20% CaO/20% Al_2O_3) in 29) indicate that a high immersion depth of the electrode into the slag contributes most strongly to a high slag skin thickness of up to 11 mm in a 268 mm mold.

However, this can be counteracted by a low slag cap thickness and a high melt current, reducing the slag skin thickness to 1 mm or below. A slag skin thickness of 0 mm, explained by the fact that a solid slag layer at the boundary between the slag cap and the mold was completely remelted at the slag/metal interface at the ingot top, was found when a low immersion depth was combined with a high slag cap height.

Modelling of the slag skin thickness is heavily influenced by the correct description of the current path, especially from the liquid slag to the mold, but the electrical conductivity of the solidified slag skin is not well-known.[30)]

1.3. Energy Dissipation in ESR:

Electroslag remelting requires significantly more energy than is necessary to melt the alloy.[15,16,22,24,26)] Different power balances were established (**Table 1**), thus the largest heat flow is towards the mold, but notably geometrical conditions have to be taken into consideration. The highest heat transfer is in the region of the slag bath followed by the heat flow from the ingot.[24,26,31–33)] In selected cases such as high slag cap height and either low immersion depth or low current operation, a strong heat transfer can also take place by radiation above the slag surface.[29)] Remelting with high resistivity low or no CaF_2-containing slags leads not only to a general reduction in energy consumption but also to a significantly lower heat transfer above and in the slag zone due to a higher thermal resistance of the slag crust.[31,32)] A similar effect can be achieved with a higher fill ratio.[16)]

Data from 29) clearly show the different effects of various operating conditions such as high/low immersion depth (Im+, Im−), high/low slag cap height (S+, S−) and high or low current (I+, I−). Thereby a rather unusual high immersion depth strongly reduces the share of heat transfer to the mold, which correlates also with a lower heat transfer above the slag bath by radiation and a lower slag temperature. A high amount of slag leads to an increase of the heat transfer at the corresponding slag region. The operation with a low melt rate results in a higher share of heat transferred to the mold, dominantly in the slag region.

The results indicate clearly that the major utilization of the electrical energy supplied to the process is actually not used for remelting, but to produce warm water at a temperature level from which it is difficult to recover significant energy. Assessing the different factors which influence and reduce energy losses, various restrictions have to be taken into account regarding their potential implementation. Fill ratios are mainly a problem in small lab-scale or multi electrode units, but are usually high in industrial production. High amounts of slag are also unusual and the melting rate is limited by the quality of the remelted ingot. New plant design such as ESRR or cooling with ionic liquids as described in 34) and 35) offer some potential, but are partly restricted to specific small sizes ingots (ESRR) and require at least partial reconstruction for existing units. Similar restrictions can be found for technologies like rotating or vibrating electrodes as described in 4), 36), 37). Therefore, changes in the slag composition towards higher resistivity and reduced thermal conductivity appear to be the most viable solutions to reduce specific energy consumption in existing ESR production.[4,5)] Such solutions, as described above, are far from new, but the application is limited. Therefore a closer examination of the achieved quality of the remelted material is necessary.

Table 1. Heat flow during ESR in % of the yielded electrical energy.

Source	Mold				Ingot (+ base plate)	Radiation losses
	Above slag	*Slag region*	*Ingot surface*	Mold total		
26)	*13*	*39*	*30*	82	18	
24)	*13*	*32*	*21*	66	9	25
24)	*17*	*32*	*27*	76	17	7
33)		*30–50*		70–80		
31,32) 0%CaF_2	*7*	*39*	*44*	90	5	
31,32) 25%CaF_2	*10*	*40*	*44*	94	5	
31,32) 50%CaF_2	*10*	*49*	*35*	94	4	
31,32) 75%CaF_2	*13*	*50*	*23*	86	3	
16) fr0.24				57	17	26
16) fr0.605				64	21	15
16) fr0.605+ lowCaF_2				63	23	14
29) S+, Im−, I+	21	41	19	81		
29) S−, Im−, I+	20	34	27	81		
29) S−, Im+, I+	15	23	23	61		
29) S+, Im+, I+	12	39	22	73		
29) S+, Im+, I−	30	51	14	95		

1.4. Effect of the Slag Composition with Low or No CaF_2-content on Cleanliness

A major reservation against the practical use of high resistivity slags result from concerns regarding negative effects on the cleanliness levels, respectively number, size and type of non-metallic inclusions, as indicated in 5). A comparison of a ball bearing steel after remelting with a standard slag of the composition 40% CaF_2, 30% CaO and 30% Al_2O_3 with several CaF_2-free slags described in 15) show that all slags had a significant cleaning effect and that good cleanliness levels can also be achieved by CaF_2-free slags with some disadvantages for high SiO_2-containing compositions. In contrast results in 18) indicate a rather limited cleaning potential of CaF_2-free slags compared to CaF_2-rich ones. A recent comparison using slag compositions (CaF_2/CaO/Al_2O_3/SiO_2/MgO) of 32-29-34-2-3% and 14-38-42-2-4% in 38) showed no negative effect of the lower CaF_2-content in the number and size of the nonmetallic inclusions. However, the higher MgO content in the slag shifted the NMI composition to spinel type inclusions of higher MgO content and a significant amount of high-MgO-inclusions. In this context it is has to be taken into consideration that the view on cleanliness has shifted over the years from sulfide removal towards oxide inclusion minimization and optimization with particular emphasis on spinel compositions.[17,38–41)]

1.5. Slag Temperature Measurement in ESR

Slag temperature measurements during remelting operation are difficult to perform and are therefore rather sparsely documented. Small scale experiments on temperature distributions and energy dissipation were conducted in 26) with a laboratory ESR-unit (mold/electrode diameter of 80/38 mm) and a slag of CaF_2 with 25% Al_2O_3. The temperature was measured using a BN sheathed W3Re-W24Re-thermocouple attached to the electrode. Typical slag temperatures with different operation modes were in the range of 1 650 to 1 780°C (~1 700°C for AC operation) and showed a constant distribution over most of the slag cap height with only some drop towards both ends, but preferentially at the last 5–10 mm towards the free slag surface, reaching 1 500–1 550°C surface temperature. Corresponding data under almost similar conditions in 27) show that slag temperatures between 1 460 and 1 720°C are possible, using pure CaF_2 but different power input. Slag temperature measurements on a similar size experimental setup reported in 31) and 32), using a W5Re-W26Re-thermocouple and various types of slags, show a strong effect of the slag composition on the temperature distribution. While the slag temperature in the core is significantly higher in the CaF_2-free slag (1 900°C) compared to a slag with 50% CaF_2 (1 790°C) the cooler areas and the slag skin at the mold wall are also much wider and thicker in the CaF_2-free slag, which can be explained by significantly different current paths, viscosity and thermal resistance of this slag.

Results from a laboratory scale protective gas ESR unit in 42), which were performed using BN protected W6Re-W26Re-thermocouples in lateral position, AC operation and a CaF_2-based slag with 30% Al_2O_3 resulted in uniform slag temperatures in center region of about 1 750°C. The temperature profile shows a significant drop to about 1 600°C at the lower 10 mm towards the metal pool and to about 1 650°C in the upper 5–10 mm at the free slag surface. Similar experiments with a slightly larger size ESR unit and vertically mounted BN shielded W-W26Re thermocouple using the same CaF_2 + 30% Al_2O_3 slag confirmed also widely constant inner slag temperatures in the range of 1 750 +/−30°C.[43] Therein temperature profiles showed no gradients towards the metal pool but a drop to below 1 500°C towards the electrode and the free slag surface. The depth of the temperature gradient is about 10 to 15 mm.

Slag temperatures for different power sources and 240 mm mold diameter using typical slags of the type (CaF_2/CaO/Al_2O_3) of 40-30-30% and 33-33-33% reported in 44) range from 1 625 to 1 780°C, with the majority of data between 1 665 and 1 760°C. Significantly higher slag temperatures of 1 700 to 1 880°C for a CaF_2-based slag with 30% CaO and Al_2O_3 each, and 1 820 up to more than 2 000°C for a slag containing 51% CaO and 49% Al_2O_3 are reported in 15) without detailed information on the position and measurement method.

According to 28) a slag temperatures of 1 700–1 725°C for the slag 60% CaF_2 + 30% Al_2O_3 and 1 650–1 675°C for the slag 60% CaF_2 + 20% CaO + 20% Al_2O_3 are suitable to produce a desired slag skin thickness of 2–3 mm for large ingots with 1 000 mm diameter. Indirect information on slag temperature can be derived from data in 22), which state an increasing overheating of 400–500°C above slag liquidus with rising ingot height. An extensive investigation of inner slag temperatures on remelting Ni-base alloy 625 with a CaF_2-based slag containing 20% CaO and Al_2O_3 each, using W5Re-W26Re-thermocuples in several depths in the annular region of the slag cap, is reported in 29). Despite using a relatively wide variety of process parameters regarding slag height, immersion depth and melt current the temperature exhibits primarily a strong linear dependency from the power input and ranges from 1 621 to 1 854°C.

Inner slag temperatures in a similar temperature range as reported from measurements were already predicted by early modelling approaches *e.g.* in 45). More advanced simulations can be used to estimate the effects of different current path, especially from the liquid slag to the mold, ingot size or frequency, indicting strong effects of these parameters,[30,46] but are usually not verified by experimental data.

Calculated slag temperatures in 46) for large molds, different frequencies and a standardized slag (50% CaF_2 - 25% CaO - 25% Al_2O_3) vary between ~1 560 and >1 600°C. In a reverse approach[47] used experimental data on slag temperatures of 1 600–1 650°C at the metal pool surface as a boundary condition for the simulation of pool profiles. In 48) the important role of slag movement due to different fill ratios and current paths towards the mold on the slag temperature distribution is pointed out. Such slag movement affects also the heat transfer to the mold and the slag skin thickness.

With all these temperature values it has to be taken into consideration that slags possess a limited partial transparency, which implies that thermocouple measurements are effected not only by the contact surface but by a certain surrounding ill-defined volume and radiation pyrometer are additionally effected by largely undefined emissivity of the surface.[6] The later case can be partially overcome with a 2-color pyrometer. Athough the power density leads to the above dependence of temperature distribution on slag resistivity, the same tendency is also supported by the changes in slag thermal conductivity due to the addition of oxides to a CaF_2 base.[19]

Generally it can be concluded that inner slag temperatures are usually in the range of 1 650 to 1 750°C but depend also strongly on the power input. The temperature distribution inside the slag but more important towards the free slag surface and the mold wall is substantially affected by the slag composition.

2. Experimental Procedure

2.1. Materials

All remelting trials were conducted using a corrosion resistant plastic mold steel of the type DIN EN X40Cr14 (AISI 420) with 0.36% C and 14.5% Cr, which was provided in the form of bright bars with a diameter of 101.5 mm. The slags used were standardized products of "Wacker Chemie AG" with the denotations ESR2015 ("30C-33A-2S-3M", CaF_2-based with ~30% CaO, ~33% Al_2O_3, ~2% SiO_2 and ~3% MgO and a calculated electrical conductivity at 1 600°C of 1.55 $\Omega^{-1}cm^{-1}$) and ESR2063 ("38C-42A-2S-4M", CaF_2-based with ~38% CaO, ~42% Al_2O_3, ~2% SiO_2 and ~4% MgO and a calculated electrical conductivity at 1 600°C of 0.99 $\Omega^{-1}cm^{-1}$). Both slags were used in a premelted granular form.

2.2. Process Parameters

For the remelting trials, a laboratory scale ESR-unit was used. The power supply, based on a Munk-D400-G100/500-WRG-SWUZ rectifier, was operated a low frequency of 4.5 Hz in open operation (no protective gas) using a slight conical round-section fixed mold with an average diameter

of 168 mm. This results in an average fill ratio of 0.37. As can be seen in **Fig. 2**, the plant is equipped with waste gas suction at the backside of the mold, almost opposite to the pyrometer, to collect evaporating fumes from above the mold. A "cold start procedure" was applied, using granular slag and 5 g of Al-granulate for initial deoxidation. Therefore, the electrode was contacted with the Al-granulate and the baseplate, forming an open arc. Subsequently the solid slag was added into the mold. During this starting period the arc does melt both the electrode and the solid slag, thereby changing the system from initial arc heating to resistance heating. The whole slag (5 kg) is typically completely melted after 15–20 min. Lower (3.5 kg, "SA-low") or higher (6.5 kg, "SA-high") amounts of slag results in an earlier (13 min) or respectively later (22 min) complete melting of the slag. Further information on the setup of the plant and low frequency operation mode can be found in.[49,50)]

The other operating parameters were adjusted to achieve constant melt rates for the slag 30C33A-2S-3M of about 50 kg/h or significantly higher ("MR-high") or lower ("MR-low") melt rates respectively 55 and 70 kg/h ("MR-high") for the slag 38C-42A-2S-4M ("low CaF_2", see also **Table 2**). The central parameter combination (5 kg of the slag 30C-33A-2S-3M and ~50 kg/h melt rate was conducted three times to demonstrate the reproducibility of the results. The voltage is mainly the result of the amount of slag, the immersion depth (1–5 mm) and the electrical conductivity of the slag. No deoxidants were added during the remelting process. The ingot length after remelting, except for "Center 1" with 370 mm) was between 450 and 520 mm. Two further experiments (Center-TC, LowCaF_2-TC) were performed using additional thermocouple measurements with interrupted remelting.

The plant is equipped with a continuous documentation of the electric energy consumption as well as a permanent measurement of the cooling water flow rate and temperature, the latter permitting an examination of the energy losses in the base plate and the mold. The evaluation of the specific energy consumption was conducted in the stable part of the process once all slag was melted, using the difference at the electricity meter ΔE in kWh, the average melt rate $MR_{average}$ in kg/h and the duration t in h of the investigated melt period according to Eq. (3), multiplied by 1 000 for conversion from kg to tonne.

$$SE = \frac{\Delta E.t}{MR_{average}} \quad \text{..... (3)}$$

2.3. Temperature Measurement

The laboratory ESR-unit is equipped with a maneuverable and compressed air cooled 2-color pyrometer (PA41AF21/S) with a measuring range of 800–2 400°C and an average spot size diameter of 5 +/−2 mm, which measures the slag surface temperature from a position above the mold (Fig. 2). Additionally, a Pt30Rh-Pt6Rh-thermocouple in an alumina tube can be positioned in the middle of the gap between the

Table 2. Process parameters of the remelting trials.

Experiment	Slag composition (remainder CaF_2)	Slag amount kg	Meltrate kg/h	Current kA	Voltage V
MR-high	30C-33A-2S-3M	5	59	3,4	62–64
SA-high	30C-33A-2S-3M	6.5	51	3,0	69–71
Center-1	30C-33A-2S-3M	5	51	3,0	63–65
Center-2	30C-33A-2S-3M	5	48	3,0	63–64
Center-3	30C-33A-2S-3M	5	50	3,0	63–65
SA-low	30C-33A-2S-3M	3.5	51	3,2	55–57
MR-low	30C-33A-2S-3M	5	37	2,6	61–64
LowCaF_2-Center	38C-42A-2S-4M	5	55	2,7	65–67
LowCaF_2-MR-high	38C-42A-2S-4M	5	73	3,25	65–68
Center-TC	30C-33A-2S-3M	5	*)	3,0	63–65
LowCaF_2-TC	38C-42A-2S-4M	5	*)	2,8	64–66

*) melting was interrupted during temperature measurements

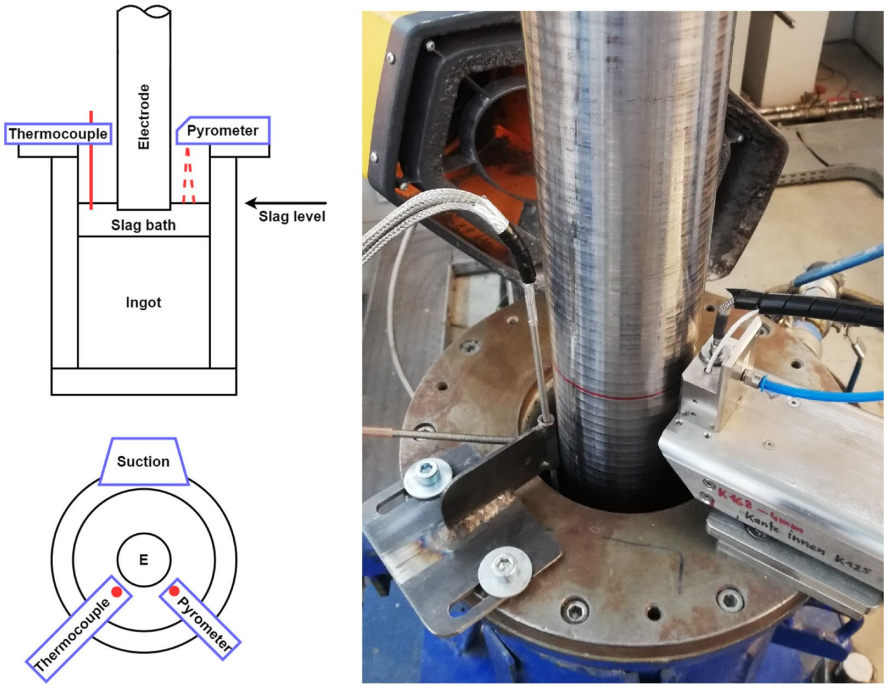

Fig. 2. Experimental set-up for the temperature measurement. (Online version in color.)

mold and the electrode. The thermocouple can be lowered or raised manually to measure the slag temperature at different slag depths and at different stages of the remelting trial. It should be emphasized that, as shown in Fig. 2, the thermocouple position and the position of the pyrometer are separated in the annular gap by 108 degree. Therefore, both measurement systems measure the slag surface temperature, but not exactly at the same location. Both, the thermocouple holder as well as the movable pyrometer were mounted at the cover plate of the mold.

The pyrometric measurements were usually set into operation 20 min after starting the experiment when full melting of the slag was achieved. Continuous temperature measurement was therefore made possible.

Two trial melts were conducted to verify and interpret the pyrometric temperature measurements by the thermocouple measurements ("Center-TC", "LowCaF_2-TC"). Therefore the thermocouple was positioned at fixed height where a liquid slag and stable melting conditions could be expected. Once the thermocouple contacted the liquid slag, remelting was continued for 20 to 40 sec to get a full immersion of the thermocouple into the slag. Then the power was turned off and after about 10 sec the thermocouple was lowered further by about 10 mm into the slag to measure the cooling of the slag. During this procedure, the slag surface temperature was continuously measured with the pyrometer for comparison.

2.4. Material Investigations

Two ingots, remelted with each of the slags, were forged and analyzed regarding their chemical composition and non-metallic inclusions. The investigation methods applied were similar to those described in 38). For this investigation, the focus was on non-metallic inclusions and their chemical composition.

The aim of this investigation was a quantified comparison of the different factors influencing the specific energy consumption of the ESR process, using one and the same equipment to determine the different energy saving potentials and to provide a first estimation on the concomitant effects on non-metallic inclusions when using different slag compositions. Additionally, a new contactless and continuously operating measurement method for the slag (surface) temperature was applied to reveal correlation with the energy consumption.

3. Results

3.1. Verification and Examination of the Temperature Measurement

Figure 3 shows the temperature curves of the thermocouple (blue) and the pyrometer (black) as a function of the process time for the verification measurement on the slag 30C-33A-2S-3M. The thermocouple measurement is affected by the 4.5 Hz current flow of the remelting process, therefore a smoothing is introduced to show the average temperature profile. The first contact point of the thermocouple is clearly visible, but it takes several seconds until the weld bead of the thermocouple is fully immersed. When the power supply of the ESR-unit was shut off, the slag tem-

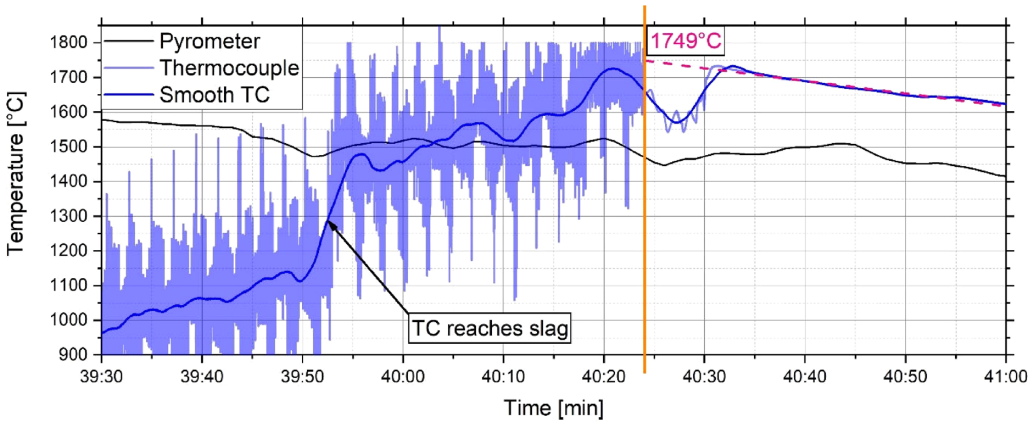

Fig. 3. Comparison of the pyrometric with the thermocouple temperature measurement in slag 30C-33A-2S-3M. (Online version in color.)

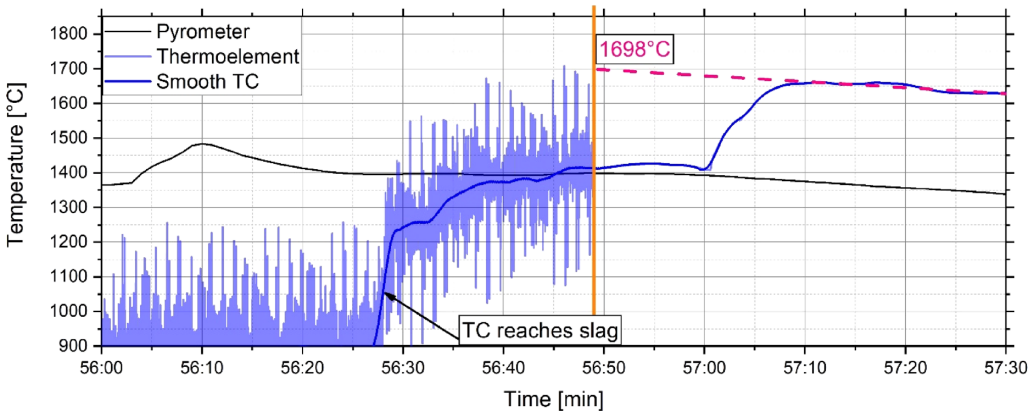

Fig. 4. Comparison of the pyrometric with the thermocouple temperature measurement in slag 38C-42A-2S-4M. (Online version in color.)

perature measured by the thermocouple was 1 657°C and cooled down to a stable temperature of just below 1 600°C after a few seconds. This is significantly warmer than the temperature of 1 462°C from the pyrometer (T_{Py}) at the same time, but at a different position. When the thermocouple was lowered by 10 mm, the measured slag temperature increased to 1 730°C. During the ongoing cooling period the temperature at the thermocouple was falling continuously, permitting the extrapolation of the slag temperature $T_{TC\text{-}10mm}$ to 1 749°C at the power turn off.

The curves of **Fig. 4** shows the results of the same procedure as in Fig. 3, but now for the slag 38C-42A-2S-4M. It is clearly recognizable that both temperature profiles, of the pyrometer as well as that of the thermocouple, are significantly lower than for the other slag. The contact point of the thermocouple is again clearly visible. After turning off the power supply the average slag surface temperature during the first second, measured by the thermocouple (T_{TC}), is 1 413°C while the pyrometrical one is 1 398°C. It has also to be taken into consideration that both temperatures are measured at different places about a quarter of the circumference apart. Lowering the thermocouple 10 mm into the slag leads to a strong increase of the slag temperature up to 1 660°C. The successive drop in temperature during the cooling period permits an extrapolation of the slag temperature $T_{TC\text{-}10mm}$ to 1 698°C.

Comparing both slags it becomes evident that, according to thermocouple measurements, slag 30C-33A-2S-3M possesses with 1 657°C a significantly higher slag surface temperature than slag 38C-42A-2S-4M with only 1 413°C. In contrast, at an immersion depth of 10 mm and extrapolated to the time of the power shut off, both slags have a significantly higher temperature and the difference (1 749 vs. 1 698°C) has become considerably smaller. These results summarized in **Table 3** indicate a much steeper temperature gradient towards the free surface in slag 38C-42A-2S-4M than in the other composition. It is also evident that there is relatively good agreement between the thermocouple and pyrometer for slag 38C-42A-2S-4M while the other slag shows a much lower pyrometer temperature.

To understand these differences, **Fig. 5** shows the complete pyrometer recordings for the experiments "Center 2" (30C-33A-2S-3M) and "LowCaF$_2$-Center" (38C-42A-2S-4M) which are typical also for the other temperature profiles of these two slags. For better comparability, the timeline was translated into the slag surface position ("slag level" in Fig. 2). Two main factors are evident: First, slag 30C-33A-2S-3M shows on the large scale a steady increase in temperature, while slag 38C-42A-2S-4M exhibits a rather constant, slightly decreasing temperature profile. Second, both slags feature fluctuations in the temperature, which are more random and oscillating for slag 30C-33A-2S-3M and repeatedly spiky in slag 38C-42A-2S-4M.

The constant temperature rise of slag 30C-33A-2S-3M can be related to the fume generated by the slag, which was observed in all experiments with this slag. As the amount of fume decreases with rising slag level, its negative effect on temperature measurement is reduced. Such fumes were not recognized at the experiments with slag 38C-42A-2S-4M, explaining the rather constant temperature trend independent of the slag level.

Some of the local temperature fluctuations of slag 30C-33A-2S-3M might also be related to an inhomogeneous fume density, but the main reason of these fluctuations can be taken from **Fig. 6** left. The surging movement of the slag leads to a cellular appearance of the slag surface, only that the colder dark area aren't completely random but can accumulate and then such cold spots move rather slowly on the surface. In contrast, the slag surface during remelting with slag 38C-42A-2S-4M basically has a much darker (colder) appearance, which is broken up from time to time by an overflow of hot slag from inside the slag pool as can be seen on Fig. 6 right. This sudden occurrence of a hot slag layer on top, followed by successive cooling, correlates directly with the spikes in the temperature profile of Fig. 5.

Table 3. Slag temperature after the turnoff of the power supply.

		T_{TC}	T_{Py}	$T_{TC\text{-}10mm}$	$T_{true\text{-}Py}$*)	ΔT_{Py}
	Time after turnoff	0–1 sec	0–1 sec	0 sec *)		
Experiment	Slag composition	°C	°C	°C	°C	°C
Center-1	30C-33A-2S-3M	–	–	–	1 655	23
Center-2	30C-33A-2S-3M	–	–	–	1 677	15
Center-3	30C-33A-2S-3M	–	–	–	1 680	18
LowCaF$_2$-Center	38C-42A-2S-4M	–	–	–	1 363	21
Center-TC	30C-33A-2S-3M	1 657	1 462	1 749	–	–
LowCaF$_2$-TC	38C-42A-2S-4M	1 413	1 398	1 698	–	–

*) extrapolated

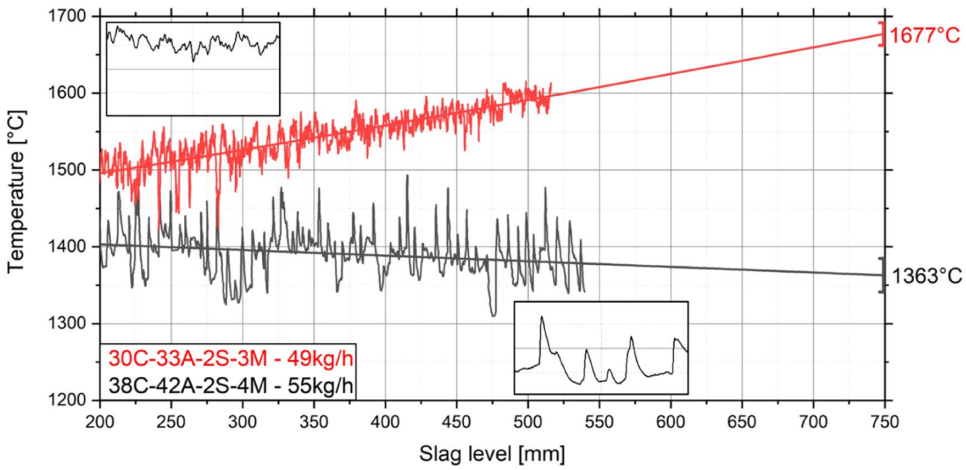

Fig. 5. Temperature profile of the slag surface temperature measured by pyrometer. (Online version in color.)

Based on this understanding, an extrapolation to a (fumeless) temperature was conducted to calculate the average temperature of the slag surface during the stable part of the remelting process ($T_{true\text{-}Py}$ in Table 3) by using the method of least squares and extrapolating the function to the upper end of the mold (Fig. 5). Furthermore, the fluctuations of the temperature profile could be used to calculate a standard deviation (ΔT_{Py}). For the mapped experiment "Center-2" in Fig. 5, this temperature $T_{true\text{-}Py}$ was 1 677°C. Retests with similar parameters resulted in $T_{true\text{-}Py}$ of 1 655 and 1 680°C, which are roughly within the standard deviation (ΔT_{Py}) of the experiments, providing reasonable repeatability. Comparing these calculated average temperatures $T_{true\text{-}Py}$ (1 655–1 680°C, ΔT_{Py} ~20°C) with the thermocouple temperature T_{TC} (1 657°C), confirms that the pyrometric temperature measurement is a useful method to monitor the slag surface temperature. Thereby it has to be taken into consideration, that also thermocouple measurements showed strong variation of the temperature after contact with the slag due to fluctuations of cold and hot areas at the slag surface.

3.2. Effect of Slag Amount

Some of the different effects of the amount of slag (30C-33A-2S-3M) for the period of stable remelting conditions are depicted in **Fig. 7**. In general, there is a weak trend towards higher values of all three parameters, slag surface temperature, specific energy consumption and slag skin thickness, with rising slag cap height. However, all changes are more or less within or only slightly above the range of scatter and reproducibility, illustrating that the effect is rather weakly developed.

Most of the energy introduced to the system is transferred to the cooling water of the mold 53.4 to 57.6% with the highest and lowest values for the highest and lowest slag amount respectively. The heat transfer towards cooling water in the base plate accounted only for 2.1 to 4.3% of the energy dissipation without any clear trend. The second highest loss of energy was detected between the power metering at the entrance of the rectifier and the power metering in the low frequency secondary circuit, accounting for power losses in the range of 30.6 to 33.1%. Excluding these power losses of the electrical power supply from the energy balance, total energy dissipation of the heat generated inside the slag towards the cooling water was between 80.8 and 90.2% with the lowest value for the lowest slag cap height, while the rest remained in the same scatter range.

3.3. Effect of the Melt Rate

In a similar way to the effect of the amount of slag, the effect of the melt rate within the parameters investigated is not very strong. As for the slag 30C-33A-2S-3M there is a general trend towards higher slag surface temperature, lower specific energy consumption and reduced slag skin thickness, whereas these trends are more strongly pronounced between 37 and 50 kg/h than at higher melt rates (**Fig. 8**). In contrast slag 38C-42A-2S-4M shows no significant effect of the melt rate on slag surface temperature or energy consumption in the investigated range, but only a reduction of the slag skin thickness by one half. More striking is the difference between the two slags with significantly lower slag surface temperature and energy consumption vales for the higher resistivity slag.

Energy dissipation to the cooling water in the mold amounted for 52.7 to 56.3% for slag 30C-33A-2S-3M and 52 to 54.1% for the slag 38C-42A-2S-4M respectively, in both cases with the lower values at the lower melt rate. Heat losses to the base plate accounted for 2.4 to 4.3% without recognizable effect of the melt rate or the slag composition. Almost the same applies to the energy losses in the rectifier, which was between 30.4 and 34.3% indicating a weak tendency towards lower values at higher melt rates. Excluding the power losses of the electrical power supply, total energy dissipation towards the cooling water was between 84.7 and 90.2% for slag 30C-33A-2S-3M and 82.3 to 82.4% for slag 38C-42A-2S-4M.

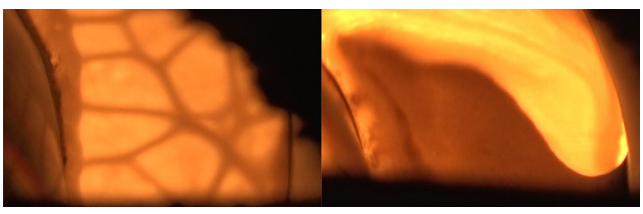

Fig. 6. Slag surface appearance during remelting, left: slag 30C-33A-2S-3M, right: slag 38C-42A-2S-4M. (Online version in color.)

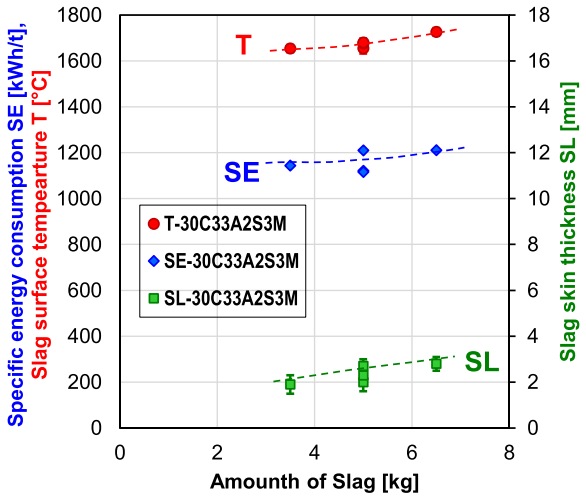

Fig. 7. Slag surface temperature, specific energy consumption and slag skin thickness as a function of the amount of slag used. (Online version in color.)

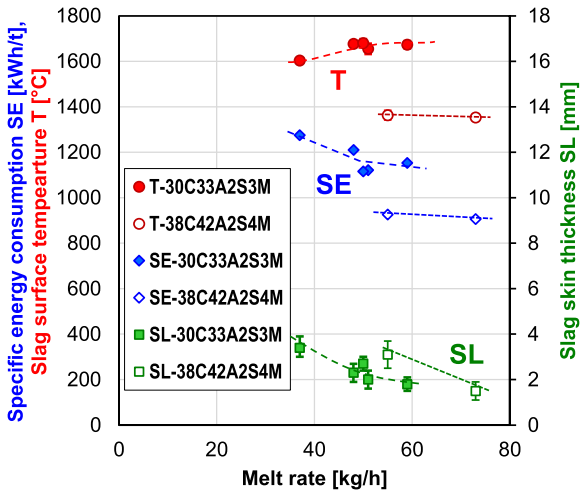

Fig. 8. Slag surface temperature, specific energy consumption and slag skin thickness as a function of the melt rate for two different slags. (Online version in color.)

3.4. Effect of the Slag Composition on Non-metallic Inclusions

The evaluation of the non-metallic inclusions (NMI) after remelting with the two different slags provided rather similar results and therefore a good cleanliness level in both remelted ingots. The total amount in area percentage was slightly lower for slag 30C-33A-2S-3M with 0.0043% than for slag 38C-42A-2S-4M with 0.0058% with the majority being oxides, some oxysulfides and almost no sulfides. This correlates well with the oxygen and sulfur contents of 8 ppm O and 5 ppm S for remelting with slag 30C-33A-2S-3M as well as 10 ppm O and 4 ppm S for slag 38C-42A-2S-4M. The composition of the NMI and its frequency can be seen in **Fig. 9** where all oxides and the oxidic part of the oxisulfides were taken into account.

The majority of the NMI were of the MA-spinel type, independent of the slag composition. However, remelting with the slag 30C-33A-2S-3M led to a second prevalent population of pure alumina type NMI. All NMI were low in their SiO_2 content. Oxy-sufides are conglomerates of MnS with the corresponding oxides.

4. Discussion

4.1. Temperature Measurement

Slag temperatures, both at the surface as well as 10 mm below the surface, determined by thermocouple measurements are in good agreement with results in 26), 27), 31), 32), 42) and 43). Thereby also the drop in temperature towards the free surface as described in 26), 31), 32), 42) and 43) were confirmed, including the effect of lower CaF_2 contents reported in 31) and 32). Additionally, the variation of the slag temperature due to its dynamic and local flow pattern demonstrate that the slags used do not have something like a homogeneous surface temperature. These local fluctuations of the surface temperature were also well detected by the pyrometric measurements, which proved to be a valid method to observe process conditions as well as differences between slags regarding their flow behavior at the free surface. However, accurate surface temperature measurements are limited by the fume between the slag surface and the pyrometer, which according to 6) and 33) is mainly caused through the evaporation of volatile fluorides according to *e.g.* Eqs. (4) and (5) and CaF_2 itself:

$$3.CaF_2 + Al_2O_3 \Leftrightarrow 3.CaO + 2.AlF_3 \quad \text{..... (4)}$$

$$2.CaF_2 + SiO_2 \Leftrightarrow 2.CaO + SiF_4 \quad \text{..... (5)}$$

As this reactions are strongly dependent on the CaF_2-content in the slag the effect is much stronger for the slag 30C-33A-2S-3M which contains roughly 32% CaF_2 compared to only 14% in slag 38C-42A-2S-4M. Continuous measurement of the slag surface temperature over a longer period of time and constant remelting parameters permitted the extrapolation of the "true" and average slag surface temperature in reasonable agreement with results from the thermocouples.

Cellular or more continuous slag surface pattern, determined both, by optical observation as well as pyrometric measurements on slag 30C-33A-2S-3M, are not uncommon for many slag types. The somehow periodic overflow behavior of slag 38C-42A-2S-4M is rather unusual and probably the result of the specific combination of a high melting point of this slag (as documented in 51)), plant size and geometry as well as corresponding current paths and inner slag movements.

4.2. Energy Consumption and Non-metallic Inclusions

As illustrated in **Fig. 10**, the specific energy consumption determined within this experimental series is in good agreement with results from laboratory as well as industrial trials of similar fill ratios from 7), 16) and 17) thereby also confirming that the fill ratio besides electrical conductivity is a main factor influencing energy consumption. However, the scatter of the experiments with varying process parameters, using the same slag 30C-33A-2S-3M with a calculated electrical conductivity of 1.55 $\Omega^{-1}cm^{-1}$, provides an indication of their potential effects.

The strong impact of the amount of slag reported in 22) and 14) could not be confirmed in this experimental series, but a weak conspiring correlation was observed. Heat losses to the cooling water tend to be higher with rising slag cap height, which corresponds to results in 29). The effect of the melt rate was found to be minor as well, lying between the results in 14) and 11), which found almost no, and 13) with a significant reduction on energy consumption with rising melt rate. The reduction in energy consumption thereby goes hand in hand with a reduction of slag skin thickness, which in the first instance looks contradictory. As reported in 27) the effect of the slag skin thickness on the energy consumption is of minor importance. Therefore, the effect of a shorter contact time due to the higher melt rate prevails.

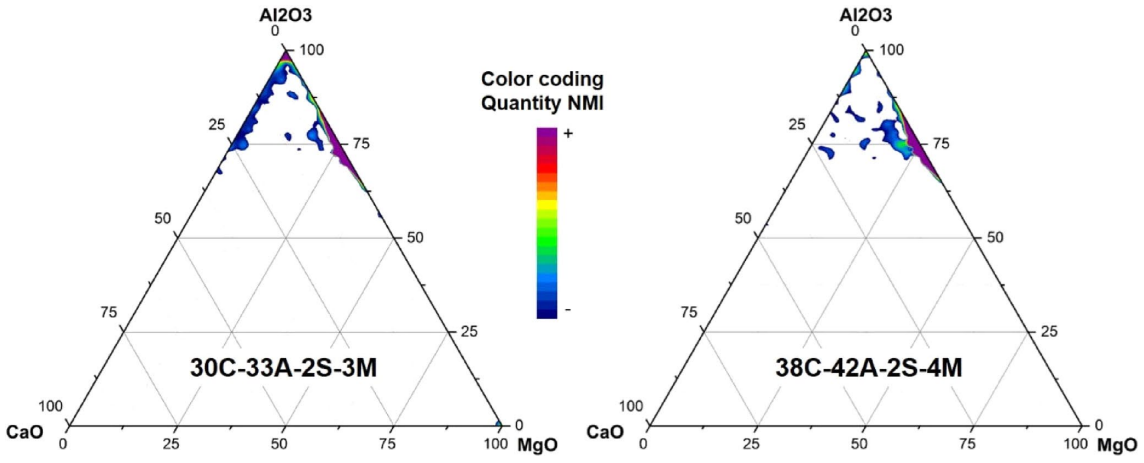

Fig. 9. Composition of the oxidic NMI after remelting with the slags 30C-33A-2S-3M (left) and 38C-42A-2S-4M (right). (Online version in color.)

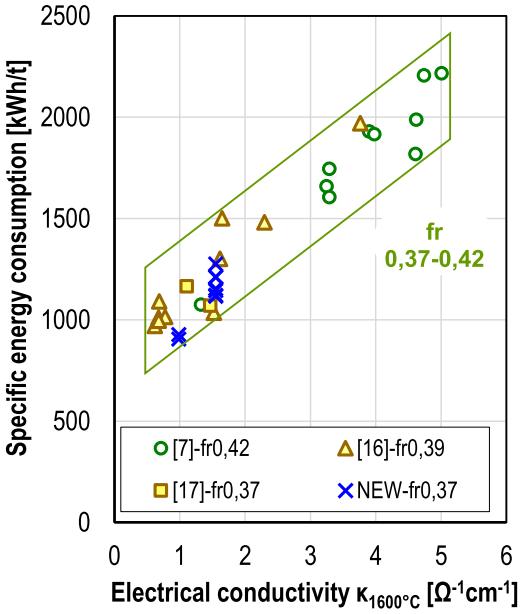

Fig. 10. Specific energy consumption as a function of the electrical conductivity at 1 600°C in comparison with results in 7), 16) and 17). (Online version in color.)

More generally, the slag skin thickness is in good agreement to published data for typical operation conditions in 22), 27) and 28).

The strongest effect on the specific energy consumption derived from this investigation, as can be seen quite clearly in Fig. 10, results from the selection of the slag composition, and thereby predominantly its electrical conductivity. Comparing the results of the two slags at similar melt rate to 50–55 kg/h, two more differences become obvious: Slag 38C-42A-2S-4M forms a much thicker slag skin and the slag surface temperature is lower by roughly 250°C. The latter significantly reduces energy losses due to heat radiation above the slag surface, which, according to 24), 26), 31), 32) and 29) account for roughly 10–20% of the energy losses. The effect of the slag skin is more complex to evaluate. As described in 2) and 29) the final slag skin at the ingot is not the same as in the slag region, but it can be assumed that they have a positive correlation towards each other, contributing to lower heat losses with rising thickness in both positions. In this specific case, using different slag compositions, also the slag skin composition will differ, leading to changes in the thermal conductivity on the slag. Variations of the slag skin thickness, and correspondingly of the temperature field inside the slag, furthermore impair the electric current flow towards the mold. This in turn affects, in combination with different viscosities of the slags, the slag movement and the heat distribution inside the slag.[26,27,31,32] The heat losses to the cooling water were slightly lower for slag 38C-42A-2S-4M, confirming the combined effects of the various parameters, but also the difficulty of separating the variables influencing the temperature distribution.

The contents of oxygen and sulfur as well as the total amount and chemical composition of the NMI are very similar to results in 38) using the same slags and detection methods, but a hot work tool steel. A small difference can only be found in the ranking, while in 38) slag 38C-42A-2S-4M had a lightly lower amount of NMI, slag 30C-33A-2S-3M performed somewhat better in this investigation, leaving the possibility that the differences of the cleanliness level are within the scatter range of sampling and detection methods. Predominantly MA-spinel type inclusions with various amounts of CaO resulting from slags with roughly 1/3 CaF_2, CaO and Al_2O_3 each are also reported in 17), 38), 40), 41) and 52). In contrast, 39) reports on predominantly alumina and calcium aluminate inclusions, but with a focus on inclusions larger 8 μm. The low SiO_2-content of the NMI correlates well with observations in 1), 17), 38) and 53) and can be explained by the low SiO_2 content of the slags used. The shift of the inclusion type to fewer pure alumina type inclusions by using the higher Al_2O_3 and higher MgO containing slag is similar to results in 17) where such slag also generated inclusions with higher MgO contents. This indicates that the rise of MgO activity is of higher importance than the corresponding rise in Al_2O_3 activity, later one in agreement with results published in 54). The lack for sulfides correlates well with the low sulfur content. More generally speaking, there seems to be no substantial negative effect on non-metallic inclusions, and therefore the cleanliness level, due to the use of the more energy efficient slag. However, more detailed investigations on the effect of the slag composition, respectively the different slag components, on the various aspects of the cleanliness level, such as amount and size distribution as well as composition and corresponding type of non-metallic inclusions, need to be conducted and will be pursued in future investigations.

5. Summary and Conclusions

- Measuring the slag surface temperature with a 2-color pyrometer proved to be a reliable method for a continuous monitoring and characterization of ESR process conditions. However, slag fume formations need to be compensated for accurate data.
- Changing the slag cap height as well as the melt rate showed only a minor effect on the slag surface temperature and the specific energy consumption, thereby demonstrating that various changes of the process conditions may compensate each other in their total effect.
- The most significant and easy to change parameter is the slag composition, thereby low-CaF_2 low-conductivity slags resulted in significantly lower slag surface temperatures and showed a significant potential to reduce total energy consumption. This effect can be related to the temperature distribution inside the remelting slag and a correspondingly reduced heat transfer to the mold by changes in the current path and thermal conductivity.
- First results on the consequences of such changes in the slag composition on non-metallic inclusions, respectively the cleanliness level after remelting are promising, but need extensive further investigations. Thereby particular attention needs to be paid on the possibilities to optimize slag compositions for specific alloys.
- Slag compositions and remelting parameters always need to be adapted to the specific quality requirements of a certain alloy and application. However, if these can be fulfilled with slags of lower conductivity, there is significant potential for energy and cost savings.
- The results also provide measured values for different parameters that can be used to validate the results of ESR models.

Acknowledgements

The authors gratefully acknowledge the funding support of K1-MET GmbH, metallurgical competence center. The research programme of the K1-MET competence center is

supported by COMET (Competence Center for Excellent Technologies), the Austrian programme for competence centers. COMET is funded by the Federal Ministry for Climate Action, Environment, Energy, Mobility, Innovation and Technology, the Federal Ministry for Digital and Economic Affairs, the Federal States of Upper Austria, Tyrol and Styria as well as the Styrian Business Promotion Agency (SFG). Beside the public funding from COMET, this research project is partially financed by scientific partners and the industrial partner voestalpine Böhler Edelstahl GmbH & CoKG.

REFERENCES

1) W. Holzgruber and E. Plöckinger: *Stahl Eisen*, **88** (1968), 638 (in German).
2) A. Mitchell: *J. Vac. Sci. Technol.*, **7** (1970), S63.
3) G. Hoyle: Electroslag Processes: Principles and Practice, Applied Science Publishers, London, (1983), 1.
4) Y.-L. Xiong, Z.-W. Song, A.-G. Wang and Y.-C. Lou: *China Foundry*, **16** (2019), 1. https://doi.org/10.1007/s41230-019-8135-5
5) S.-C. Duan and H.-J. Guo: *Steel Res. Int.*, **91** (2020), 1900634. https://doi.org/10.1002/srin.201900634
6) A. Mitchell: Proc. 2005 Int. Symp. on Liquid Metal Processing and Casting (LMPC 2005), (Santa Fe), ASM International, Materials Park, (2005).
7) J. Korp: Ph.D. thesis, Montanuniversität Leoben, (2007), https://pure.unileoben.ac.at/portal/files/2490551/AC06520032n01vt.pdf, (accessed 2021-10-10) (in German).
8) J. Korp, R. Schneider, P. Presoly and W. Krieger: *BHM Berg-Hüttenmänn. Monatsh.*, **153** (2008), 175 (in German).
9) P. Presoly, J. Korp and R. Schneider: *Arch. Metall. Mater.*, **53** (2008), 1.
10) S. Hara, H. Hashimoto and K. Ogino: *Trans. Iron Steel Inst. Jpn.*, **23** (1983), 1053.
11) S. F. Medina and M. P. de Andrés: *Rev. Metal.*, **19** (1983), 271 (in Spanish).
12) G. Jeszensky, T. Kajita, J. D. W. Rawson and A. W. Bryant: Proc. 39th Cong. Anual, Vol. 2, (Belo Horizonte), ABM, São Paulo, (1984), 211 (in Portuguese).
13) T. El Gammal and F. A. Denkhaus: *Stahl Eisen*, **109** (1989), 1171 (in German).
14) T. El Gammal and I. von Hagen: Grundlagen der Raffination eines einfachen Baustahles nach dem Elektro-Schlacke-Umschmelzverfahren, Forschungsbericht des Landes Nordrhein-Westfalen Nr. 2565, Westdeutscher Verlag, Opladen, (1976), 1 (in German).
15) G. Brückmann and K. Schwerdtfeger: *Stahl Eisen*, **103** (1983), 387 (in German).
16) Z. Li, J. Zhang, J. Jiang and W. Cui: Proc. 7th Int. Conf. on Vacuum Metallurgy, Special Meltings and Metallurgical Coatings (ICVM), Iron and Steel Institute of Japan, Tokyo, (1982), 1486.
17) R. Schneider, C. Schüller, P. Würzinger, G. Reiter and C. Martinez: *BHM Berg-Hüttenmänn. Monatsh.*, **160** (2015), 117 (in German).
18) W. E. Anable, R. H. Nafziger and D. C. Robinson: *J. Met.*, **25** (1973), 55.
19) A. Mitchell and K. Kelkar: *Ironmaking Steelmaking*, **48** (2021), 1151. https://doi.org/10.1080/03019233.2021.1948317
20) C. Chen and R. Gao: *Acta Metall. Sin.*, **24** (1988), 221 (in Chinese).
21) M. Wahlster and E. Zimmermann: *Radex-Rundsch.*, (1973), 379 (in German).
22) P. Dewsnap and R. Schlatter: Proc. 5th Int. Symp. on Electroslag and Other Special Melting Technologies, (Pittsburgh), (1974), 91.
23) W. Holzgruber, K. Petersen and P. E. Schneider: Transaction of the Int. Vacuum Metallurgy Conf., (Beverly Hills), American Vacuum Society, New York, (1968), 499.
24) W. Holzgruber: *Radex-Rundsch.*, (1975), 409 (in German).
25) H. Jäger and G. Kühnelt: *BHM Berg-Hüttenmänn. Monatsh.*, **120** (1975), 423 (in German).
26) A. Mitchell and S. Joshi: *Metall. Trans.*, **4** (1973), 631.
27) A. Mitchell and S. Joshi: *Metall. Trans.*, **2** (1971), 449.
28) R. Schumann and C. Ellebrecht: Proc. 5th Int. Symp. on Electroslag and Other Special Melting Technologies, (Pittsburgh), (1974), 180.
29) J. E. Heilman and B. K. Damkrober: Proc. Int. Symp. on Liquid Metal Processing and Casting, (Santa Fe), (1994), 143.
30) A. Kharicha, E. Karimi-Sibaki, M. Wu, A. Ludwig and J. Bohacek: *Steel Res. Int.*, **89** (2018), 1700100. https://doi.org/10.1002/srin.201700100
31) T. Kusamichi, T. Ishii, T. Onoye and K. Narita: *Tetsu-to-Hagané*, **66** (1980), 1640 (in Japanese).
32) T. Kusamichi, T. Ishii, T. Makino, T. Onoye and K. Narita: Proc. 7th Int. Conf. on Vacuum Metallurgy: Special Meltings and Metallurgical Coatings (ICVM), Iron and Steel Institute of Japan, Tokyo, (1982), 1503.
33) A. Mitchell and R. M. Smailer: *Int. Met. Rev.*, **24** (1979), 231.
34) W. Holzgruber and H. Holzgruber: *Iron Steelmaker*, **25** (1998), 107.
35) M. Kubin, B. Ofner, H. Holzgruber, R. Schneider, D. Enzenhofer, A. Filzwieser and S. Konetschnik: Proc. 2015 Int. Symp. on Liquid Metal Processing and Casting (LMPC 2015), IOP, Bristol, UK, (2015), 28.
36) I. V. Chumanov and V. I. Chumanov: *Metallurgist*, **45** (2001), 125.
37) C. Demicri, B. Mellinghoff, J. Schlüter, C. Wissen, M. Schwenk and B. Friedrich: Proc. Liquid Metal Processing and Casting Conf. (LMPC 2019), (Birmingham), TMS, Pittsburgh, PA, (2019), 117.
38) R. Schneider, M. Molnar, S. Gelder, G. Reiter and C. Martinez: *Steel Res. Int.*, **89** (2018), 1800161. https://doi.org/10.1002/srin.201800161
39) E. Sjöqvist Persson, A. Karasev, A. Mitchell and P. G. Jönsson: *Metals*, **10** (2020), 1620. https://doi.org/10.3390/met10121620
40) Y.-W. Dong, Z.-H. Jiang, Y.-L. Cao, A. Yu and D. Hou: *Metall. Mater. Trans. B*, **45** (2014), 1315.
41) H. Wang, C.-M. Shi, J. Li, C.-B. Shi and Y.-F. Qi: *Ironmaking Steelmaking*, **45** (2018), 6. https://doi.org/10.1080/03019233.2016.1235078
42) Y. Oguti, Y. Tanbe, S. Miyama and A. Ejima: *Tetsu-to-Hagané*, **63** (1977), 2152 (in Japanese).
43) M. Kawakami, K. Nagata, M. Yamamura, N. Sakata, Y. Miyashita and K. S. Goto: *Tetsu-to-Hagané*, **63** (1977), 2162 (in Japanese).
44) G. Brückmann, G. Sick and K. Schwerdtfeger: *Metall. Trans. B*, **14** (1983), 761.
45) J. Kreyenberg and K. Schwerdtfeger: *Arch. Eisenhuettenwes.*, **50** (1979), 1.
46) A. J. Elliot, K. M. Kelkar, C. O. Miller, J. D. Naumann and R. J. Roberts: Proc. Liquid Metal Processing & Casting Conf. 2017 (LMPC 2017), (Philadelphia), TMS, Pittsburgh, PA, (2017), 205.
47) A. S. Ballantyne and A. Mitchell: *Ironmaking Steelmaking*, **4** (1977), 222.
48) A. Mitchell: *Mater. Sci. Eng. A*, **413**–**414** (2005), 10.
49) R. Schneider, A. Paar, P. Zeller, G. Reiter, W. Schützenhöfer and P. Würzinger: *BHM Berg- Hüttenmänn. Monatsh.*, **156** (2011), 112 (in German). https://doi.org/10.1007/s00501-011-0636-5
50) R. Schneider, M. Mülleder, P. Zeller, P. Würzinger, G. Reiter and S. Paul: *BHM Berg- Hüttenmänn. Monatsh.*, **161** (2016), 20. https://doi.org/10.1007/s00501-016-0462-x
51) A. Mitchell: *Can. Metall. Q.*, **20** (1981), 101.
52) A. Paar, R. Schneider, P. Zeller, G. Reiter, S. Paul and P. Würzinger: *Steel Res. Int.*, **85** (2014), 570. https://doi.org/10.1002/srin.201300317
53) M. Allibert, J. F. Wadier and A. Mitchell: *Ironmaking Steelmaking*, **5** (1978), 211.
54) M. Hino, S. Kinoshita, H. Ito and S. Yorozuya: *CAMP-ISIJ*, **7** (1994), 41 (in Japanese).